

A Numerical Evaluation of SAR Distribution and Temperature Changes Around a Metallic Plate in the Head of a RF Exposed Worker

Robert L. McIntosh,^{1*} Vitas Anderson,² and Raymond J. McKenzie¹

¹Telstra Research Laboratories, Clayton, Australia

²EME Australia, Frankston, Australia

The 1998 International Commission for Non-Ionising Radiation (ICNIRP) Guidelines for human exposure to radiofrequency (RF) fields contain a recommendation to assess the potential impact of metallic implants in workers exposed up to the allowable occupational field limits. This study provides an example of how numerical electromagnetic (EM) and thermal modelling can be used to determine whether scattered RF fields around metallic implants in workers exposed to allowable occupational ambient field limits will comply with the recommendations of relevant standards and guidelines. A case study is performed for plane wave exposures of a 50 mm diameter titanium cranioplasty plate, implanted around 5–6 mm under the surface of the forehead. The level of exposures was set to the ambient power flux density limits for occupational exposures specified in the 1998 ICNIRP guidelines and the current 1999 IEEE C95.1 standard over the frequency range 100–3000 MHz. Two distinct peak responses were observed. There was a resonant response for the whole implant at 200–300 MHz where the maximum dimension of the implant is around a third of the wavelength of the RF exposure. This, however, resulted in relatively low peak specific energy absorption rate (SAR) levels around the implant at the exposure limits. Between 2100–2800 MHz, a second SAR concentrating mechanism of constructive interference of the wave reflected back and forth between the air-scalp interface and the scalp-plate interface resulted in higher peak SARs that were within the allowable limits for the ICNIRP exposures, but not for the IEEE C95.1 exposures. Moreover, the IEEE peak SAR limits were also exceeded, to a lesser degree, even when the implant was not present. However, thermal modelling indicated that the peak SAR concentrations around the implant did not result in any peak temperature rise above 1 °C for occupational exposures recommended in the ICNIRP guidelines, and hence would not pose any significant health risk. Bioelectromagnetics 26:377–388, 2005. © 2005 Wiley-Liss, Inc.

Key words: occupational radiofrequency exposure; safety standards; cranioplasty; metallic implants; Pennes bioheat equation; finite difference

INTRODUCTION

Whenever a person is exposed to a radiofrequency (RF) field, currents and fields will be induced inside the body that will heat tissue due to dielectric losses. The International Commission for Non-Ionising Radiation (ICNIRP) recommend that RF induced tissue temperature rises do not exceed 1 °C [ICNIRP, 1998], and adherence to exposure limits in international RF safety standards [IEEE, 1999] and guidelines [ICNIRP, 1998] are generally assumed to ensure this.

A fundamental metric for specifying RF heating is the specific energy absorption rate (SAR) expressed as W per kg of tissue mass. SAR can be calculated at any point in the exposed tissue from knowledge of the internal electric field (E) using:

$$\text{SAR} = \frac{\sigma |E|^2}{\rho}$$

where σ is the conductivity (S/m), ρ is the mass density (kg/m³), and E is expressed in rms V/m. When setting protective limits for localised tissue heating, the point SAR is mass averaged, in recognition of the thermal diffusion properties of tissues. The averaging mass in ICNIRP [1998] is any 10 g of contiguous

Grant sponsor: Asian Office for Aerospace Research and Development (AOARD) of the United States Air Force Office of Scientific Research (AFOSR).

*Correspondence to: Robert L. McIntosh, Telstra Research Laboratories, 770 Blackburn Rd, Clayton VIC 3168, Australia. E-mail: robert.l.mcintosh@team.telstra.com

Received for review 18 February 2004; Final revision received 8 February 2005

DOI 10.1002/bem.20112

Published online 27 May 2005 in Wiley InterScience (www.interscience.wiley.com).

tissue. The IEEE [1999] standard specifies a smaller 1 g averaging mass in the shape of a cube, though it is expected that a 10 g cubic averaging mass will be specified in the next edition [IEEE, 2004].

Because SAR is difficult to measure or calculate, RF safety is most often determined by compliance with the more practical metrics of ambient electric and magnetic field exposure limits, often expressed in terms of equivalent plane-wave power flux density (W/m^2). As with the averaging masses, the formulation of these ambient field limits varies somewhat between different standard setting bodies. For example, the IEEE limits differ from the ICNIRP guidelines in both the maximum level specified ($100 \text{ W}/\text{m}^2$ for IEEE and $50 \text{ W}/\text{m}^2$ for ICNIRP) and the frequency at which these peak values are reached (2000 MHz for ICNIRP and 3000 MHz for IEEE). A trade-off for using ambient field limits is the necessity to set these limits conservatively in order to cater for the many different possible combinations of exposures (e.g., field polarisation, subject grounding and size), which can substantially influence RF power absorption. The field exposure limits have been designed to ensure compliance with whole body average SAR restrictions. It has been generally assumed that these exposure limits will also ensure compliance with *localised* SAR restrictions though this has not been comprehensively proven. In particular, the ability of metallic objects implanted inside the body to scatter and concentrate RF fields at certain points around them requires further investigation.

There are many people who carry metallic items inside their bodies. Such items include shrapnel as well as medical implants including orthopaedic plates, screws, wires and rods, and electronic devices such as pacemakers. Whenever a RF field impinges on such a metallic object, the field is scattered around the conductor and may redistribute the energy of the incident field to produce significant peak SAR concentrations around certain parts of the implant. ICNIRP [1998] specifically recommends that such persons occupationally exposed to high fields should be assessed for the potential to exceed allowable localised SAR limits. A more fundamental consideration is whether a possible resultant temperature increase arising from the redistributed SAR would exceed a generally acceptable benchmark level of 1°C (see the discussion presented in ICNIRP [1998]). Setting this value as a threshold for a local peak is conservative given that the body can support a 1°C rise in the core temperature.

This study explores the use of RF and thermal modelling techniques for assessing metallic implants via a particular example of a titanium cranioplasty plate surgically implanted in the forehead. Such plates are used to repair a defect in the skull resulting from an

accident, an operation (such as tumor removal), or skull malformation. Using numerical techniques, the SAR distribution around the implant and the consequent temperature rise are calculated.

This study follows that of Cooper and Hombach [1996], who studied an implanted metallic plate in the head using a simple homogeneous spherical model of the head with a dipole to simulate a mobile phone at the single frequency of 900 MHz. They raised the concern that the presence of such an implant "... can enhance local values of SAR considerably... although the presence of implantations should seldom be a risk." Other implants such as auditory implants, heart stents, pacemakers, wires and rods have previously been considered in, for example, Hocking et al. [1991]; Fleming et al. [1992, 1999]; Chou et al. [1995, 1997]; Foster et al. [1999]; DeMarco et al. [2002]; Lazzi et al. [2002]; and Scanlon [2004].

This study is confined to the analysis of occupational far-field RF exposure. Thus no conclusions may be drawn from the results of this work from near-field RF exposures such as might be experienced by mobile phone users.

ELECTROMAGNETIC (EM) MODELLING METHODOLOGY

Computational Setup

Induced SAR in the human body was calculated using the commercially available finite-difference time-domain (FDTD) software, XFDTD [Remcom, Inc., 2004]. The ability of FDTD methods to handle the highly irregular and heterogeneous structures in the human anatomy has made it a popular choice in human SAR modelling (see, e.g., Taflove and Brodwin [1975]; Kunz and Luebbers [1993]; Guy et al. [2002]).

A realistic three-dimensional full-body finite-difference geometry based on the Visible Human [National Library of Medicine, 2004] has been constructed at the Brooks Air Force Base, United States Air Force [Brooks AFB, 2004]. Remcom, Inc. has provided the full-body geometry in a form that can be used by XFDTD. The human head geometry consists of the twenty-three tissues listed in Table 1. Extra tissues present in the body geometry, but not in the head, are the bladder, bile, body fluids, gall bladder, small and large intestine, kidneys, liver, inner and outer lung, toe and finger nails, spleen, and stomach. The dielectric properties (electrical conductivity σ and relative permittivity ϵ_r) and mass densities (ρ) used in this study were specified by Brooks AFB who primarily used the data from Gabriel [1996]. Examples of this data are presented in Table 1 for the frequencies 200 MHz

TABLE 1. Dielectric Properties at 200 and 2500 MHz and Density of Head Tissues and Titanium Cranioplasty Plate

Tissue and plate	200 MHz		2500 MHz		Density (kg/m ³)	Source
	σ (S/m)	ϵ_r	σ (S/m)	ϵ_r		
Blood	1.28	68.5	2.59	58.2	1058	a
Blood vessel walls	0.51	51.1	1.47	42.5	1040	b
Bone marrow (red)	0.03	5.9	0.10	5.3	1040	a
Cancellous bone	0.20	24.4	0.82	18.5	1920	a
Cartilage	0.52	49.2	1.79	38.7	1097	a
Cerebellum	0.90	67.1	2.13	44.7	1038	a
Cerebro-spinal fluid	2.19	76.8	3.50	66.2	1007	a
Cortical bone	0.07	13.9	0.40	11.4	1990	a
Eye cornea	1.10	65.3	2.33	51.5	1076	a
Eye lens (cortex)	0.63	50.5	1.53	44.6	1053	a
Eye sclera	0.94	61.2	2.07	52.6	1026	a
Eye vitreous humour	1.51	69.0	2.52	68.2	1008	a
Fat	0.04	5.7	0.11	5.3	916	a
Glands	0.83	64.1	2.01	57.1	1050	a
Grey matter	0.64	65.1	1.84	48.8	1038	a
Ligaments	0.52	49.4	1.73	43.0	1220	a
Lymph nodes	0.83	64.1	2.01	57.1	1040	b
Mucous membrane	0.59	55.7	1.62	42.8	1040	b
Muscle	0.74	60.2	1.77	52.7	1046	a
Nerve (spinal chord)	0.39	39.7	1.11	30.1	1038	a
Skin	0.58	55.7	1.49	38.0	1125	a
Tooth	0.07	13.9	0.40	11.4	2160	b
White matter	0.38	47.1	1.24	36.1	1038	a
Air	0	1	0	1	1.16	c
Titanium alloy	5.9×10^5	1	5.9×10^5	1	4700	d

^aDielectric properties from Gabriel [1996], densities from Brooks AFB [2004].

^bBrooks AFB [2004].

^cDensity from Gandhi et al. [2001]. 'Air' has been included in the geometry in the internal head cavities for thermal modelling purposes.

^dAutomation Creations [2004].

and 2500 MHz (two important frequencies in the following discussion). For other frequencies see Gabriel [1996] and Brooks AFB [2004].

The EM excitation used throughout this study is a uniform plane-wave, incident on the front of the body. The E field is parallel to the long axis of the body producing the highest coupling of the field with the human body at VHF frequencies and below. Such a field would simulate an RF worker in the far-field of a radiating source (such as a mobile phone base station) and looking directly at the source.

THERMAL MODELLING METHODOLOGY

A finite difference model based upon Pennes' bioheat equation [Pennes, 1948] has been developed to determine the localised temperature increase, T , in the human model due to SAR. See examples of the use of the equation and related discussion in Bernardi et al. [1998, 2000]; Van Leeuwen et al. [1999]; Wang and Fujiwara [1999]; Gandhi et al. [2001]. Pennes' equation is of the form

$$\rho c \frac{\partial T}{\partial t} = \nabla \cdot (K \nabla T) + \rho \text{SAR} + A_0 - b(T - T_b) \quad (1)$$

where c is the specific heat capacity, K is the thermal conductivity, A_0 is the metabolic heat production, b is the heat-sink strength from each tissue volume by blood perfusion and T_b is the temperature of blood. The thermal conditions at the surface of the body are modelled as a convective boundary:

$$K \frac{\partial T}{\partial n} = -h(T - T_a) \quad (2)$$

where h is the convection coefficient, T_a is the ambient temperature and n is the unit normal to the surface. The desired solution for T is obtained when the system reaches steady-state. The finite-difference model that was developed is based on the formulation of Bernardi et al. [2003]. This formulation also addresses thermo-regulatory effects such as sweating. The program can use the SAR calculated by XFDTD as an input, and the results can also be viewed by XFDTD. A validation study, based upon the comparison with an analytic

solution for a “muscle” cylinder, as presented in Bernardi et al. [1998] was successfully completed. Further confidence in the program was provided through experimental measurements that were in agreement with the thermal model results for a study performed in McIntosh et al. [2003].

In this study, the temperature of blood, T_b , was chosen to be 37 °C, and the ambient temperature, T_a , was set to 20 °C. The convection coefficient h was chosen to be 10.5 W/m²·°C as in Wang and Fujiwara [1999] (who reference Kritikos et al. [1981]). To reduce the substantial computational requirements, the thermal modelling was performed in the head and shoulder region of the body mesh (which is appropriate since we are looking for small localised changes around the position of the plate). At the base of the head and shoulder mesh (where it is detached from the body) the ambient temperature, T_a , is given the temperature of blood, T_b . The convection coefficient, h , was chosen to be 2 W/m²·°C as this value gives a thermal profile in this region that best approximates the expected profile in a full human body model (following the method of Bernardi et al. [2000]).

The thermal properties of each tissue and the plate are listed in Table 2. Values for c have no impact on the final steady-state solution since c is the coefficient of the time derivative of the temperature T in Pennes’ equation. Cavities inside the head model (e.g., in the mouth, pharynx, and sinuses) were given the thermal properties of air.

In Pennes’ temperature formulation, blood is generally viewed as perfusing all tissues and its heat transfer contribution is represented by the $b(T-T_b)$ term. As in references Bernardi et al. [1998, 2000], blood is only considered as a separate entity if it is present in large vessels or in regions where blood pools are present. Examples of large vessels in the XFDTD model of the Visible Human head include the jugular vein and the carotid artery. In these cases, a forced convective boundary condition was applied to tissue surfaces adjacent to the blood using a high h term (see also Legendijk [1982]). However, the technique and level of accuracy of the modelling of the large blood vessels actually had very limited influence on the calculated temperature profile in the region surrounding the plate. For a more complete treatment of the vascular system see, for example, Van Leeuwen et al. [1999].

The temperature increase due to the induced SAR is determined by subtracting the calculated ‘basal’ temperature profile, where there is no input SAR, from the temperature profile when the SAR is present.

ANALYSIS AND RESULTS

The human body model, used in both the RF and thermal analyses, comprised cubical finite-difference mesh cells of length 2.0 mm. This mesh size was retained for all frequencies considered. A 50 mm diameter titanium cranioplasty plate, 2.0 mm or one cell thick, was incorporated into the forehead of the mesh around 5–6 mm under the surface (see Figs. 1 and 2). Wherever possible, each mesh cell that comprised the plate was chosen to replace the outermost cell that represented cortical bone. The holes and screws in the plate were not included in the model.

SAR and temperature profiles for the head with and without the implanted plate were calculated for several frequencies between 100 and 3000 MHz at a constant uniform ambient power flux density of 10 W/m², and also at the occupational field exposure limits specified in ICNIRP [1998] and IEEE [1999] for the relevant frequencies.

Baseline SAR and Temperature Increase for the Head Without the Plate

SAR and temperature results for the head prior to the plate being implanted are presented in Table 3 as a baseline reference. The peak SARs in these models occurred near the nose except at the lower frequencies where they occurred in the spinal column or the muscular region of the jaw. The peak localised temperature rise surpasses 1 °C at both 2400 and 3000 MHz for the IEEE [1999] limits.

Basal Temperature Profiles

The average basal temperature of the head (with or without plate) was calculated to be 36.28 °C with a maximum temperature of 37.18 °C recorded in the grey matter. The only noticeable differences in temperature profiles between the head with the plate compared to the head without the plate occur in a small region of a few millimetres about the position of the plate. In particular, the plate and the tissue directly adjacent to the plate are up to a peak of 0.57 °C cooler than the corresponding region in the head without the plate. This is in part due to the significantly higher thermal conductivity, K , of the plate that results in a more effective heat conductance path from the nearby deeper parts of the head to the surface. To a lesser degree it is also because the plate has replaced a small volume of tissue (apart from the cortical bone) that has non-zero blood perfusion and metabolic heat production values (Table 2). This cooling impact of the plate would be expected to offset SAR induced temperature rises.

TABLE 2. Thermal Properties of Tissues and Titanium Cranioplasty Plate*

Tissue and plate	c specific heat capacity (J/kg · °C)	K thermal conductivity (W/m · °C)	b heat-sink strength from tissue volume by blood perfusion (W/m ³ · °C)	A_0 ^a metabolic heat production (W/m ³)
Blood vessel walls ^b	3553	0.46	9000	1600
Bone marrow (red) ^c	2700	0.22	28230	5020
Cancellous bone ^d	2150	0.30	14120	2510
Cartilage ^e	3586	0.50	60	10
Cerebellum ^f	3687	0.57	56490	10040
Cerebro-spinal fluid ^g	3934	0.56	0	0
Cortical bone ^d	1650	0.30	0	0
Eye cornea ^h	4200	0.58	0	0
Eye lens (cortex) ⁱ	3000	0.50	0	0
Eye sclera ^e	4200	0.54	0	0
Eye vitreous humour ⁱ	4200	0.60	0	0
Fat ^j	2393	0.23	1020	220
Glands ^k	3686	0.49	24410	4340
Grey matter ^l	3687	0.57	56490	10040
Ligaments ^m	2802	0.31	4830	860
Lymph nodes ⁿ	3686	0.49	31800	5650
Mucous membrane ^h	3300	0.43	9000	1600
Muscle ^j	3634	0.55	2140	380
Nerve (spinal chord) ^c	3500	0.46	11440	2030
Skin ^j	3610	0.42	12310	2190
Tooth ^o	1340	0.50	0	0
White matter ^l	3600	0.50	15890	2820
Air ^p	1008	0.03	0	0
Titanium alloys ^q	525	7.00	0	0

*In cases where more than one source was provided for each tissue property, the average values were used. Either the thermal conductivity, K , or the specific heat capacity, c , may in some cases be derived from values given for the thermal diffusivity, $\alpha = K/\rho \cdot c$, where the density, ρ , is listed in Table 1. The value for b was often derived from the blood flow rate.

^aAll values of A_0 were chosen as in Bernardi et al. [2003], that follows the suggestion in Gordon et al. [1976] that metabolic heat production is proportional to blood perfusion.

^b c and K originate from the values given for the human aorta in Van Gemert et al. [1986], Valvano and Chitsabesan [1987], and Duck [1990]; b was set to be equivalent to the value for mucous membrane.

^cBernardi et al. [2003] (c and K); b originates from Cowles et al. [1971].

^dBiyikli et al. [1986] provided c and K for cortical and cancellous bone; for cancellous bone b was set to be the average of cortical bone (i.e. zero) and bone marrow.

^eGandhi et al. [2001] (c , K , b) and Bernardi et al. [2003] (c and K).

^fThe properties for cerebellum were set to be equivalent to those for grey matter.

^gVan Leeuwen et al. [1999], Gandhi et al. [2001], and Bernardi et al. [2003].

^hBernardi et al. [2003].

ⁱVan Leeuwen et al. [1999].

^jSeveral references including Bard [1961] (b), Chato [1966] (c and K), Cowles et al. [1971] (b), Bowman [1981] (K), Williams and Leggett [1989] (b), Duck [1990] (c , K , b), Guyton [1991] (b), Wang and Fujiwara [1999] (c , K , b), Van Leeuwen et al. [1999] (c , K , b), Gandhi et al. [2001] (c , K , b), and Bernardi et al. [2003] (all).

^kProperties for the glands were averaged from the values of pituitary, pineal and parotid glands in Bernardi et al. [2000] and Gandhi et al. [2001].

^l c and K originate from Cooper and Trezek [1972], Van Leeuwen et al. [1999], and Bernardi et al. [2003]. The values for b are available from many sources including Gupta [2004].

^mHoque and Gandhi [1988] and Bernardi et al. [2003].

ⁿ c and K were set to be equivalent to those for glands; b originates from Cowles et al. [1971] and Williams and Leggett [1989].

^o c originates from Duck [1990], and K from Soyenkoff and Okun [1958] and Craig and Peyton [1961].

^pGandhi et al. [2001].

^qAutomation Creations [2004].

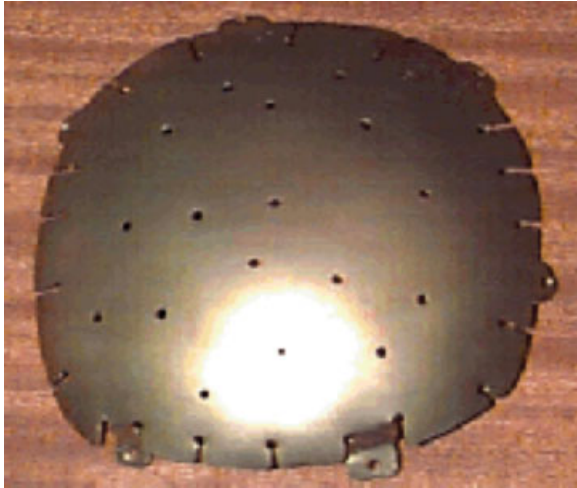


Fig. 1. A titanium cranioplasty plate [University College London, 2004].

EM Effects With the Presence of the Plate

With the presence of the plate, there are two main EM effects that can be observed—a resonance effect (occurs around 200–300 MHz) and a constructive interference effect (2100–2800 MHz). For a uniform ambient power flux density of 10 W/m^2 , the peak unaveraged SAR reaches 7.64 W/kg at 200 MHz, and 4.50 W/kg at 2500 MHz. These effects are discussed in further detail in the following two sections.

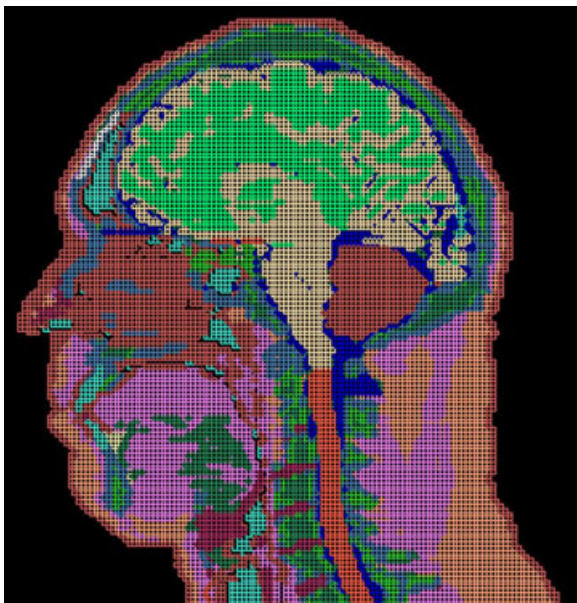


Fig. 2. Central cross-sectional slice of the head region of the mesh of the visible human body with the titanium cranioplasty plate (white cells) incorporated into the forehead.

Increased SAR and Temperature Due to the Resonance Effect

In the frequency range 200–300 MHz, the wavelength in the scalp is approximately 170 mm, which is near resonance for the plate (the diameter is around a third of a wavelength). The increased SAR is due to an enhanced E field at the ends of this antenna-like structure (see Fig. 3). Figure 4 shows the SAR levels at the bottom of the plate and the resultant temperature increase. With respect to the correspondence between SAR estimates and temperature rises, the 10 g averaged SAR most closely matches the scale of variation in the temperature rise curve. For the SAR levels produced by the resonance effect at 200 MHz, the local temperature rise is at most $0.09 \text{ }^\circ\text{C}$ at both the ICNIRP and IEEE occupational exposure limits. This is lower than the highest local temperature rise in the head due to SAR, calculated to be $0.23 \text{ }^\circ\text{C}$ in the jaw.

Increased SAR and Temperature Due to the Constructive Interference Effect

In the frequency range 2100–2800 MHz, the thickness of the scalp in front of the plate of around 5–6 mm corresponds to a distance of around a quarter wavelength. As a result (see, e.g., Ramo et al. [1984]), there is a constructive interference of the wave reflected back and forth between the air-scalp interface and the scalp-plate interface. Thus the highest SAR values are concentrated in front of the plate (see Fig. 5).

See Figure 6 for the SAR levels at the front of the plate and for the resultant temperature increase. In ICNIRP [1998], the SAR averaging mass is specified as any 10 g of contiguous mass. For the higher frequency range in which the constructive interference effect dominates, the contiguous mass that produces the highest peak SAR values takes the form of a ‘pancake’-like shape in the scalp in front of the plate. To accommodate this, and to also provide a comparison between different averaging shapes, the peak SAR values are presented in Figure 6a,b for both the cube and the pancake shapes. For frequencies outside of the 2100–2800 MHz range, the pancake shape is not relevant.

The highest peak temperature increase is $0.46 \text{ }^\circ\text{C}$ at 2600 MHz for the ICNIRP [1998] limits, and $0.80 \text{ }^\circ\text{C}$, also at 2600 MHz, for the IEEE [1999] limits (Fig. 6d). When the plate is not present, the peak increases at the same frequency of 2600 MHz are only slightly lower at $0.43 \text{ }^\circ\text{C}$ for ICNIRP [1998] and $0.75 \text{ }^\circ\text{C}$ for IEEE [1999] which were both situated at the top of the nose (Table 3). The volume or shape of the SAR averaging mass has no impact on the temperature calculation, making this a more robust metric on which to base this type of

TABLE 3. Peak SAR Values and Resultant Peak Temperature Increase in the Head (Without the Plate) for Plane-Wave Exposures at ICNIRP [1998] Occupational and IEEE [1999] C95.1 Controlled Field Exposure Limits*

Frequency (MHz)	ICNIRP 98			IEEE C95.1		
	Field exposure limit (W/m ²)	Peak 10 g cube SAR (W/kg)	Peak temperature increase (°C)	Field exposure limit (W/m ²)	Peak 1 g cube SAR (W/kg)	Peak temperature increase (°C)
100	10	0.21 ^a	0.04 ^a	10	0.37 ^a	0.04 ^a
200	10	0.81 ^b	0.23 ^b	10	1.43 ^b	0.23 ^b
300	10	0.32 ^a	0.08 ^b	10	0.50 ^b	0.08 ^b
400	10	0.43 ^a	0.09 ^b	13.3	1.07 ^b	0.12 ^b
500	12.5	0.45 ^b	0.09 ^b	16.7	0.87 ^b	0.12 ^b
600	15	0.77 ^b	0.17 ^b	20	1.81 ^b	0.23 ^b
900	22.5	1.91	0.24	30	3.96	0.32
1200	30	2.99	0.43	40	7.93	0.57
1500	37.5	3.67	0.55	50	9.90	0.73
1800	45	3.05 ^b	0.65 ^b	60	6.57 ^b	0.86 ^b
2100	50	3.47 ^b	0.69 ^b	70	8.90	0.97 ^b
2200	50	3.52	0.65 ^b	73.3	9.79	0.96 ^b
2300	50	3.99	0.60	76.7	12.54	0.92
2400	50	4.87	0.64	80	17.72	1.03
2500	50	4.77	0.58	83.3	17.24	0.97
2600	50	3.58	0.43	86.7	13.18	0.75
2700	50	2.76	0.43	90	10.36	0.77
2800	50	2.77	0.50	93.3	10.53	0.92
3000	50	3.86	0.69	100	16.48	1.38

*In this table, the peak SAR values and temperature increase values occurred near the nose unless otherwise specified.

^aThe peak occurred in the spinal column.

^bThe peak occurred in the jaw.

analysis. Figure 7 plots the increase in temperature due to SAR for the case where the frequency is 2500 MHz.

Due to the cooling effect of the plate noted earlier, the resultant absolute temperature around the plate under both sets of power flux density limits is still, on average, lower for the head with the plate when compared to the head without the plate, at all frequencies considered.

The constructive interference effect can best be analysed using semi-analytic tools such as provided by Yang and Thompson [1996]. This numerical program calculates the propagation and absorption of a plane-wave in infinite multi-layer planar geometries with the incident plane-wave normal to each surface. In particular, the analysis highlights the high level of absorption in the scalp and the low level of reflection back into the air. The program was used to confirm that the constructive interference effect is accentuated in the 2100–2800 MHz range for the plate depth of around 5–6 mm. The program is helpful in showing the level of absorption for different parameters such as materials, frequencies and depth of implant under the skin. Since exposure limits change with frequency, it does not necessarily follow that the highest SAR levels from this behaviour will occur at the depth of precisely a quarter wavelength.

Comparison With the SAR Limits

The ICNIRP [1998] occupational spatial peak SAR limit in the head is 10 W/kg for a 10 g mass. These limits are not exceeded with the presence of the plate (Fig. 6b). At the ICNIRP field exposure limits, the highest peak SAR adjacent to the plate is obtained at 2600 MHz where the peak SAR is 6.63 W/kg for the 10 g pancake-like shape (compared with 4.57 W/kg for the 10 g cube at 2500 MHz). The highest peak 10 g average SAR (calculated in the shape of a cube) for the head prior to the insertion of the plate is 4.87 W/kg obtained at 2400 MHz (this peak is obtained at the bottom of the nose).

The IEEE [1999] ‘occupational’ (controlled environment) spatial peak SAR limit in the head is 8 W/kg for a 1 g mass (the averaging mass is in the shape of a cube). When the plate is present, this limit is exceeded, in the tissue adjacent to the plate, in the range 2100–2800 MHz (Fig. 6b) for the IEEE occupational field limits. At 2600 MHz, the peak 1 g average SAR adjacent to the plate of 16.76 W/kg is double the IEEE [1999] occupational limit. It can also be observed in Table 3 that even if the head plate is not present, the peak 1 g SAR in the head is in excess of the allowable limit at 1500 MHz and in the range 2100–3000 MHz, reaching

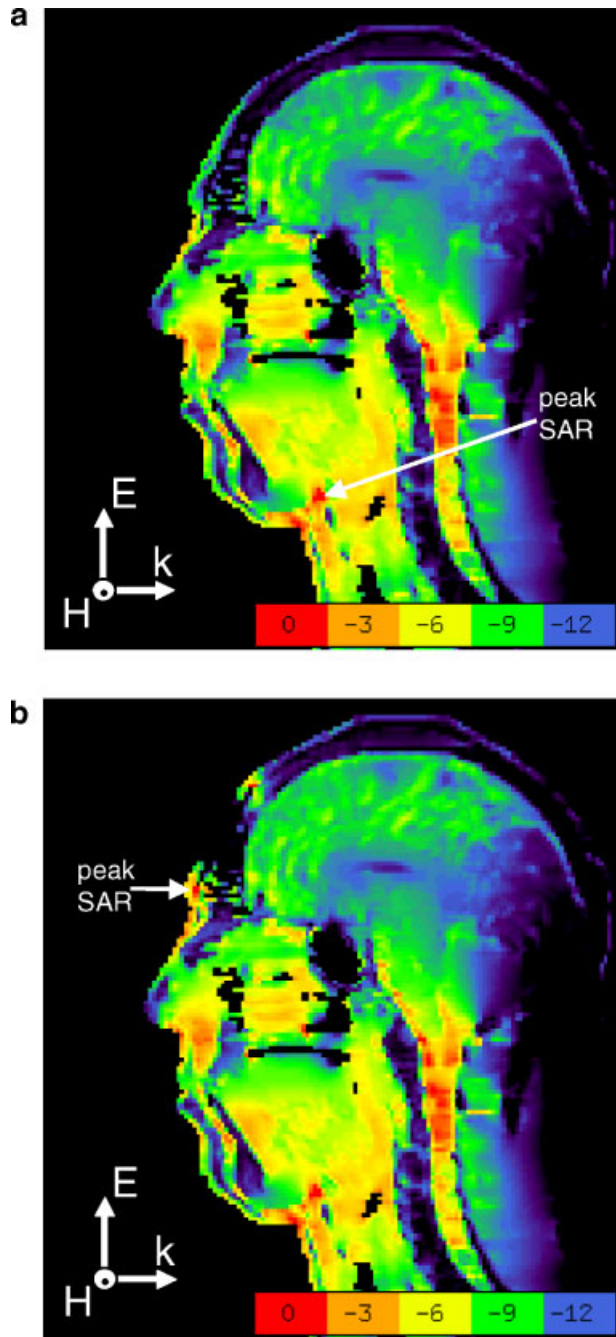


Fig. 3. SAR at 200 MHz in the central cross-sectional slice of the head for an incident power flux density of 10 W/m^2 : (a) without the plate (the peak unaveraged SAR = 3.49 W/kg and is situated in the jaw); (b) with the plate (the peak unaveraged SAR = 7.64 W/kg and is situated underneath the plate). The scale is a dB scale, with $0 \text{ dB} = 5.0 \text{ W/kg}$, and areas in the head without colour are areas with negligible SAR or there is no tissue present.

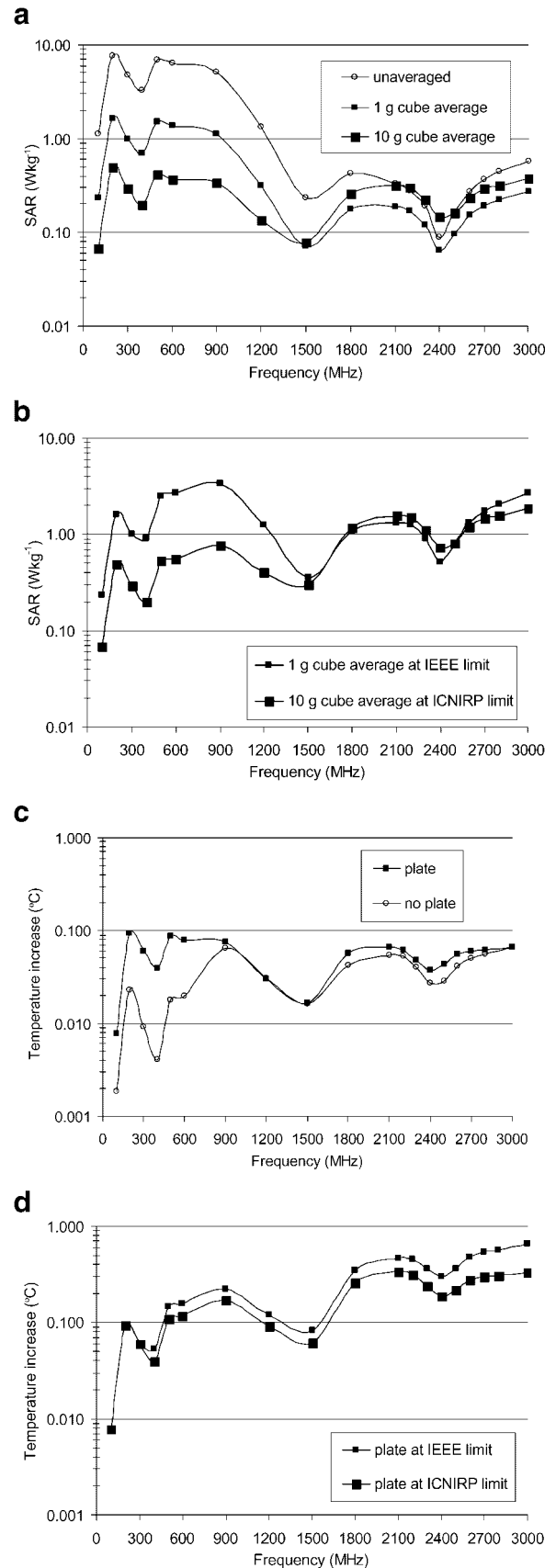


Fig. 4.

17.72 W/kg at 2400 MHz (obtained near the bottom of the nose).

In both cases, the presence of the plate does not lead to significantly higher peak 1 g or peak 10 g average SAR values in the head (when calculated in the shape of a cube), compared to when the plate is not present.

DISCUSSION

Observations From the Modelling With the Plate Present

The analysis in this study has shown that for this case study, whilst significant SAR levels may be present, the resultant temperature increase near the plate has not exceeded the limit of 1 °C recommended in ICNIRP [1998].

For other configurations of cranioplasty plates, similar numerical modelling can be used to determine whether an RF worker that has such an implant will comply with the relevant safety standard. The depth of the scalp above the plate is unlikely to be much less than the 5–6 mm in the example presented in this study. Thus the frequency at which the constructive interference effect occurs is unlikely to occur at much greater than 2800 MHz. Furthermore, it also follows that the peak SAR values are not likely to significantly exceed those presented in this study.

In ICNIRP [1998], the SAR averaging mass is specified as any 10 g of contiguous mass. In the higher frequency range, the contiguous mass that produces the highest peak SAR values in this study takes the form of a ‘pancake’-like shape in front of the plate. Indeed, the results in Figure 6a,b show that the pancake averaging mass gives peak 10 g SAR values that are up to 75% higher than for the cubical averaging mass. However, this elongated shape does not properly reflect the thermal diffusion properties of blood perfused tissues.

The SAR and temperature plots in Figure 4 appear to indicate that the cubical 10 g average SAR best represents the scale of resultant temperature increase (comparing the SAR and temperature profiles next to the plate in Fig. 4a with Fig. 4c, and Fig. 4b with Fig. 4d). This observation is in accordance with general advice provided in a 1993 NRPB Board Statement [McKinlay et al., 1993].

Fig. 4. SAR and temperature increase near the bottom of the plate: (a) SAR for an incident field of 10 W/m²; (b) SAR at the ICNIRP [1998] and IEEE [1999] field limits; (c) temperature increase for an incident field of 10 W/m²; (d) temperature increase at the ICNIRP [1998] and IEEE [1999] field limits. The data for these figures were recorded at a region near the bottom of the plate at which the peak was reached at 200 MHz (see Fig. 3b).

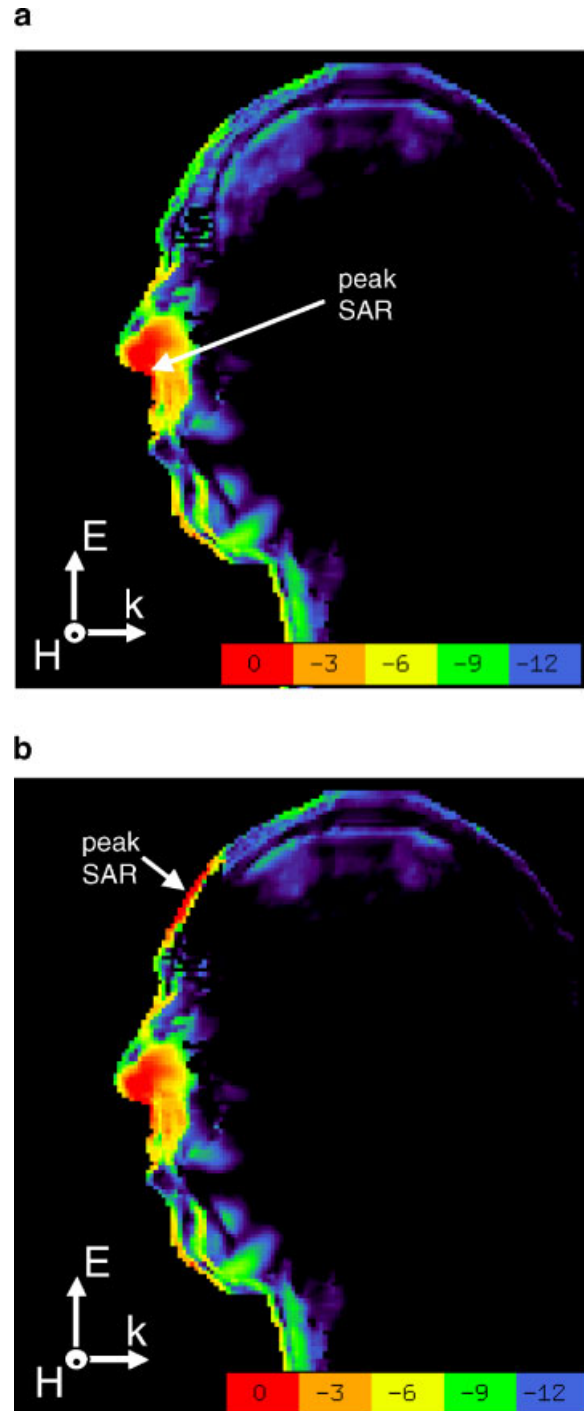


Fig. 5. SAR at 2500 MHz in the central cross-sectional slice of the head for an incident power flux density of 10 W/m²: (a) without the plate (the peak unaveraged SAR = 2.23 W/kg and is situated at the top of the nose); (b) with the plate (the peak unaveraged SAR = 4.50 W/kg and is situated in front of the plate). The scale is a dB scale, with 0 dB = 5.0 W/kg, and areas in the head without colour are areas with negligible SAR or there is no tissue present.

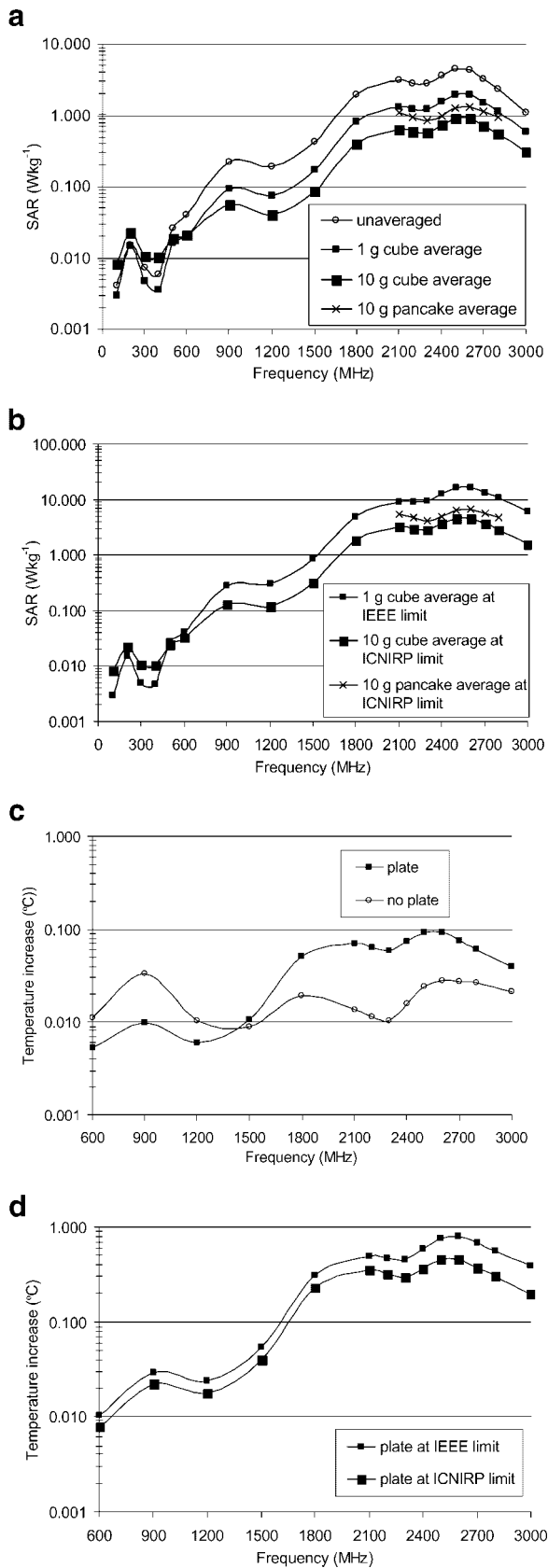


Fig. 6.

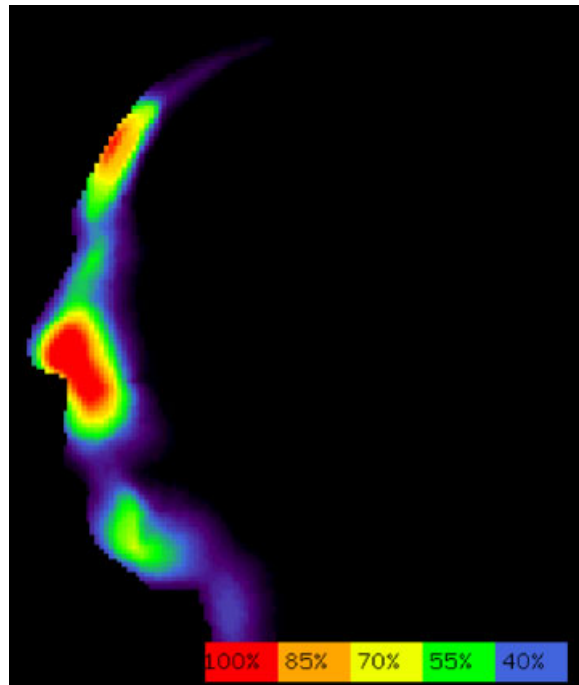


Fig. 7. Central cross-sectional slice of the temperature increase in the head (with plate) due to the input SAR at 2500 MHz. The scale is linear and the peak temperature increase is 0.46 °C at the ICNIRP [1998] limit of 50 W/m² and 0.80 °C at the IEEE [1999] limit of 83.3 W/m².

Observations From General Human Body Modelling (With the Plate Not Present)

That the IEEE [1999] limits appear to be exceeded even when the plate is not present suggests that the limits are not formulated as conservatively as intended. It was also observed that the peak localised temperature rise surpasses 1 °C at both 2400 and 3000 MHz for the IEEE [1999] limits. In the full body model, the calculated whole body average SAR is 0.20 W/kg at 2500 MHz (for the ambient field limit of 83.3 W/m²), well under the limit of 0.4 W/kg. However, the peak 1 g average SAR in the head is 17.2 W/kg (at the base of the nose), more than two times above the localised SAR limit of 8 W/kg. These calculated values suggest that the actual ratio of localised peak SAR to whole body average SAR is much higher than both the ratio of 20 (8 W/kg:0.4 W/kg) assumed in IEEE [1999] and the

Fig. 6. SAR and temperature increase in front of the plate: (a) SAR for an incident field of 10 W/m²; (b) SAR at the ICNIRP [1998] and IEEE [1999] field limits; (c) temperature increase for an incident field of 10 W/m²; (d) temperature increase at the ICNIRP [1998] and IEEE [1999] field limits. The data for these figures were recorded at a region in the scalp, near the centre of the plate, at which the peak was reached at 2500 MHz (see Fig. 5b). Note that the 1 and 10 g SAR averaging cubes overlap the plate. The temperature values for frequencies below 600 MHz are not presented due to their insignificance.

ratio of 25 (10 W/kg:0.4 W/kg) assumed in ICNIRP [1998]. Certainly, there have been no substantiated cases of harm arising from exposure at the maximum field limits permissible in either IEEE or ICNIRP, the basic principles of which have been observed for decades. The lack of significant temperature effects described here confirms that no harmful effect is likely to occur. If any conclusion may be drawn, it is that there appears to be an inconsistency between the stated formulation of the limits and what is observed in theoretical studies such as this. Moreover, this has only become apparent since the recent developments in EM modelling techniques have enabled placing these long standing principles under such detailed scrutiny. For similar conclusions from other studies see Dimbylow [2002], which states that the ICNIRP reference levels "... may not be sufficiently conservative in the region approaching 3 GHz," and Bernardi et al. [2003].

CONCLUSION

In this study, it has been shown how EM and thermal modelling can be used to calculate quantitative estimates of SAR and temperature increases around metallic objects implanted in the body, and thereby determine compliance with safety standards and guidelines for human exposures to RF fields.

A case study was presented of a 50 mm diameter titanium cranioplasty plate, implanted around 6 mm under the surface of the forehead under a plane-wave excitation, propagating towards the front of the human body. Two mechanisms for enhancing SAR near the implant were identified. First, at 200–300 MHz, SAR concentrations at the ends of the plate implant (parallel to the electric field) were caused by a resonance response of the whole implant. Second, at 2100–2800 MHz, there is constructive interference of the incident wave in the scalp with the wave reflected off the planar metallic implant. When the incident exposure level was set to the controlled environment *E* field limits of the IEEE [1999] standard, the peak spatial SAR limit (8 W/kg over 1 g) was exceeded in the frequency range 2100–2800 MHz. However, thermal analyses indicated an acceptable peak temperature increase in the scalp in front of the plate of at most 0.80 °C. Of interest, it was also found that the peak spatial SAR limit of the IEEE [1999] standard (8 W/kg over 1 g) was also exceeded in the same frequency range without the implant present. Field exposures at the reference levels of the ICNIRP [1998] guidelines for RF workers did not induce localised SAR levels that exceeded the 10 W/kg 10 g average SAR limit at all frequencies considered, and the peak temperature increase was at most 0.46 °C. Given the lack of any localised temperature increase of over

1 °C around the metallic plate implant considered in this study, it is concluded that it poses no safety risk for persons exposed up to the controlled environment or occupational field limits of the IEEE [1999] standard and ICNIRP [1998] guidelines.

ACKNOWLEDGMENTS

Dr. Anderson is supported in this study Asian Office for Aerospace Research and Development (AOARD) of the United States Air Force Office of Scientific Research (AFOSR).

REFERENCES

- Automation Creations, Inc. 2004. Matweb—Material Property Data. Available from: <http://www.matweb.com/> [Last accessed 20 Jan 2004].
- Bard P. 1961. Medical physiology, 11th edition. St Louis: Mosby.
- Bernardi P, Cavagnaro M, Pisa S, Piuze E. 1998. SAR distribution and temperature increase in an anatomical model of the human eye exposed to the field radiated by the user antenna in a wireless LAN. *IEEE Trans Microwave Theory Techniques* 46:2074–2082.
- Bernardi P, Cavagnaro M, Pisa S, Piuze E. 2000. Specific absorption rate and temperature increases in the head of a cellular-phone user. *IEEE Trans Microwave Theory Techniques* 48:1118–1126.
- Bernardi P, Cavagnaro M, Pisa S, Piuze E. 2003. Specific absorption rate and temperature elevation in a subject exposed in the far-field of radio-frequency sources operating in the 10–900-MHz range. *IEEE Trans Biomedical Eng* 50:295–304.
- Biyikli S, Modest MF, Tarr R. 1986. Measurements of thermal properties for human femora. *J Biomed Mat Res* 20:1335–1345.
- Bowman HF. 1981. Heat transfer and thermal dosimetry. *J Microwave Power* 16:121–133.
- Brooks Air Force Base, United States Air Force. 2004. FDTD geometries of the Visible Human. Available from: ftp://starview.brooks.af.mil/EMF/dosimetry_models/computer_coded_binary_files/man/ [Last accessed 20 Jan 2004].
- Chato JC. 1966. A survey of thermal conductivity and diffusivity data on biological materials. *ASME 66-WA(HT-37):1–9*.
- Chou CK, McDougall JA, Chan KW. 1995. Absence of radio-frequency heating from auditory implants during magnetic resonance imaging. *Bioelectromagnetics* 16:307–316.
- Chou CK, McDougall JA, Chan KW. 1997. RF heating of implanted spinal fusion stimulator during magnetic resonance imaging. *IEEE Trans Biomed Eng* 44:367–373.
- Cooper J, Hombach V. 1996. Increase in specific absorption rate in human heads arising from implantations. *Electron Letts* 32:2217–2219.
- Cooper TE, Trezek GJ. 1972. A probe technique for determining the thermal conductivity of tissue. *J Heat Transfer Trans ASME* 94:133–140.
- Cowles AL, Borgstedt HH, Gillies AJ. 1971. Tissue weights and rates of blood flow in man for the prediction of anesthetic uptake and distribution. *Anesthesiology* 35:523–526.
- Craig RG, Peyton FA. 1961. Thermal conductivity of tooth structure, dental cements, and amalgam. *J Dent Res* 40:411–418.
- DeMarco SC, Lazzi G, Liu W, Weiland JD, Humayun MS. 2003. Computed SAR and thermal elevation in a 0.25 mm 2d model

- of the human eye and head in response to an implanted retinal stimulator—Part I: Models and methods. *IEEE Trans on Ant and Prop* 51:2274–2285.
- Dimbylow PJ. 2002. Fine resolution calculations of SAR in the human body for frequencies up to 3 GHz. *Phys Med Biol* 47:2835–2846.
- Duck FA. 1990. Physical properties of tissue—A comprehensive reference book. Cambridge: Academic Press.
- Fleming AHJ, Lubinas V, Joyner KH. 1992. Calculation of electric fields in tissue near metallic implants. *Proceedings 1992 Asia-Pacific Microwave Conference, IEEE.*
- Fleming AHJ, Anderson V, Rowley JR. 1999. Computational estimate of the frequency response of metallic implants in biological tissues exposed to RF fields. *Proceedings 1999 ACES Annual Review of Progress in Applied Computational Electromagnetics.*
- Foster KR, Goldberg R, Bonsignore C. 1999. Heating of cardiovascular stents in intense radiofrequency magnetic fields. *Bioelectromagnetics* 20:112–116.
- Gabriel C. 1996. Compilation of the dielectric properties of body tissues at RF and microwave frequencies. *Brooks Air Force Technical Report AL/OE-TR-1996-0037*; 1996. Available from: <http://www.fcc.gov/fcc-bin/dielec.sh/> [Last accessed 20 Jan 2004].
- Gandhi O, Li Q-X, Kang G. 2001. Temperature rise for the human head for cellular telephones and for peak SARs prescribed in safety guidelines. *IEEE Trans Microwave Theory Techniques* 49:1607–1613.
- Gordon RG, Roemer RB, Horvath SM. 1976. A mathematical model of the human temperature regulatory system—Transient cold exposure response. *IEEE Trans Biomed Eng BME* 23:434–444.
- Gupta N. 2004. *NeuroReview—An educational resource for medical trainees and professionals providing concise information on topics in the clinical neurosciences.* Available from: <http://www.ucsf.edu/nreview/> [Last accessed 20 Jan 2004].
- Guy AW, Chou CK, Bit-Babik G. 2002. FDTD derived SAR distributions in various size human head models exposed to simulated cellular telephone handset transmitting 600 mW at 835 MHz. Presentation at 2002 Bioelectromagnetics Society Conference, Quebec City, Canada.
- Guyton AC. 1991. *Textbook of medical physiology.* Philadelphia: Saunders.
- Hocking B, Joyner KH, Fleming HJ. 1991. Implanted medical devices in workers exposed to radio-frequency radiation. *Scand J Work Environ Health* 17:1–6.
- Hoque M, Gandhi OP. 1988. Temperature distributions in the human leg for VLF-VHF exposures at the ANSI-recommended safety levels. *IEEE Trans Biomed Eng* 35:442–449.
- Institute of Electrical and Electronics Engineers, Inc. 1999. *IEEE Std C95.1 (1999): IEEE standard for safety levels with respect to human exposure to radio frequency electromagnetic fields, 3 kHz to 300 GHz.* New York: Institute of Electrical and Electronics Engineers.
- Institute of Electrical and Electronics Engineers, Inc. 2004. *IEEE C95.1/D1.8 (2004): IEEE standard for safety levels with respect to human exposure to radio frequency electromagnetic fields, 3 kHz to 300 GHz.* New York: Institute of Electrical and Electronics Engineers.
- International Commission on Non-Ionizing Radiation Protection. 1998. Guidelines for limiting exposure to time-varying electric, magnetic, and electromagnetic fields (up to 300 GHz). *Health Phys* 74:494–522.
- Kritikos HN, Foster KR, Schwan HP. 1981. Temperature profiles in spheres due to electromagnetic heating. *J Microwave Power* 16:327–344.
- Kunz KS, Luebbers RJ. 1993. *The finite difference time domain method for electromagnetics.* Boca Raton: CRC Press.
- Legendijk JJW. 1982. The influence of bloodflow in large vessels on the temperature distribution in hyperthermia. *Phys Med Biol* 27:17–23.
- Lazzi G, DeMarco SC, Liu W, Weiland JD, Humayun MS. 2003. Computed SAR and thermal elevation in a 0.25 mm 2-d model of the human eye and head in response to an implanted retinal stimulator—Part II: Results. *IEEE Trans on Ant and Prop* 51:2286–2295.
- McIntosh RL, McKenzie RJ, Iskra S, Carratelli A, Standaert P. 2003. Computation of SAR in cell culture flasks exposed to 900 MHz GSM type signals in a modified TEM cell. *Appl Comput Electromagn Soc J* 18:107–113.
- McKinlay AF, Allen SG, Dimbylow PJ, Muirhead CR, Saunders RD. 1993. Board statement on restrictions on human exposure to static and time varying electromagnetic fields and radiation. National Radiological Protection Board (NRPB). Documents of the NRPB, 4 No. 5.
- National Library of Medicine. 2004. *The Visible Human Project.* Available from: http://www.nlm.nih.gov/research/visible/visible_human.html/ [Last accessed 20 Jan 2004].
- Pennes HH. 1948. Analysis of tissue and arterial blood temperatures in the resting human forearm. *J Appl Physiol* 1:93–122.
- Ramo S, Whinnery JR, Van Duzer T. 1984. *Fields and waves in communication electronics.* 2nd edition. New York: John Wiley and Sons. 287p.
- Remcom, Inc. Welcome to Remcom. 2004. 2004. Available from: <http://www.remcom.com/> [Last accessed 20 Jan 2004].
- Scanlon WG. 2004. RF safety considerations for bodyworn and body-implanted radiators. Available from: http://group.ieee.org/groups/scc28/scanlon_pres_ICES0602.ppt/ [Last accessed 20 Jan 2004].
- Soyenkoff BC, Okun JH. 1958. Thermal conductivity measurements of dental tissues with the aid of thermistors. *J Amer Dental Assoc* 57:23–30.
- Taflove A, Brodwin ME. 1975. Computation of the electromagnetic fields and induced temperatures within a model of the microwave-irradiated human eye. *IEEE Trans Microwave Theory Techniques* 23:888–896.
- University College London and UCL Hospitals, Medical Graphics and Imaging Group. 2004. *Medical Physical Services.* Available from: <http://www.medphys.ucl.ac.uk/mgi/service.htm/> [Last accessed 20 Jan 2004].
- Valvano JW, Chitsabesan B. 1987. Thermal conductivity and diffusivity of arterial wall and atherosclerotic plaque. *Lasers Life Sci* 1:219–229.
- Van Gemert MJC, Welch AJ, Bonnier JJM, et al. 1986. Some physical concepts in laser angioplasty. *Semin Interv Radiol* 3:27–38.
- Van Leeuwen GMJ, Legendijk JJW, Van Leersum BJAM, Zwamborn APM, Hornsleth SN, Kotte ANTJ. 1999. Calculation of change in brain temperatures due to exposure to a mobile phone. *Phys Med Biol* 44:2367–2379.
- Wang J, Fujiwara O. 1999. FDTD computation of temperature rise in the human head for portable phones. *IEEE Trans Microwave Theory Techniques* 47:1528–1534.
- Williams LR, Leggett RW. 1989. Reference values for resting blood flow to organs of man. *Clinical Phys Physiol Meas* 10:187–217.
- Yang YS, Thompson CJ. 1996. *PlaneEMR software.* Dept of Mathematics, University of Melbourne.